J Comput Neurosci (2012) 32:55–72
DOI 10.1007/s10827-011-0339-7

Coarse-grained event tree analysis for quantifying Hodgkin-Huxley neuronal network dynamics

Yi Sun · Aaditya V. Rangan · Douglas Zhou · David Cai

Received: 23 February 2011 / Revised: 28 April 2011 / Accepted: 28 April 2011 / Published online: 20 May 2011

Abstract We present an event tree analysis of studying the dynamics of the Hodgkin-Huxley (HH) neuronal networks. Our study relies on a coarse-grained projection to event trees and to the event chains that comprise these trees by using a statistical collection of spatial-temporal sequences of relevant physiological observables (such as sequences of spiking multiple neurons). This projection can retain information about network dynamics that covers multiple features, swiftly and robustly. We demonstrate that for even small differences in inputs, some dynamical regimes of HH networks contain sufficiently higher order statistics as reflected in event chains within the event tree analysis. Therefore, this analysis is effective in discriminating small differences in inputs. Moreover, we use event trees to analyze the results computed from an efficient library-based numerical method proposed in our previous work, where a pre-computed high resolution data library of typical neuronal trajectories during the interval of an action potential (spike) allows us to avoid resolving the spikes in detail. In this way, we can evolve the HH networks using time steps one order of magnitude larger than the typical time steps used for resolving the trajectories without the library, while achieving comparable statistical accuracy in terms of average firing rate and power spectra of voltage traces. Our numerical simulation results show that the library method is efficient in the sense that the results generated by using this numerical method with much larger time steps contain sufficiently high order statistical structure of firing events that are similar to the ones obtained using a regular HH solver. We use our event tree analysis to demonstrate these statistical similarities.

Keywords Event tree analysis · Information transmission · Hodgkin-Huxley neuronal network · Library method · Neuronal coding

Action Editor: David Terman

Y. Sun (✉)
Statistical and Applied Mathematical Sciences Institute, 19 T.W. Alexander Drive, P.O. Box 14006, Research Triangle Park, NC 27709, USA
e-mail: yisun@samsi.info

A. V. Rangan · D. Cai
Courant Institute of Mathematical Sciences and Center for Neural Science, New York University, New York, NY 10012, USA

D. Zhou · D. Cai
Department of Mathematics and Institute of Natural Sciences, Shanghai Jiao Tong University, Shanghai, 200240, People's Republic of China

1 Introduction

Animals can respond to noisy stimulus swiftly within a few 100 ms (Roitman and Shadlen 2002; Uchida and Mainen 2003; Rousselet et al. 2003; Abraham et al. 2004; Mainen 2006; Uchida et al. 2006). How the brain encodes sensory information in such a short time is a fundamental question in neuroscience. In other words, what are the mechanisms by which the brain extracts the salient features of noisy input reliably and robustly? To effectively capture the relevant information about the input from the whole spatiotemporal history of the high-dimensional network dynamics, there is a need

to understand coarse-grained projection mechanisms to lower dimensions. The firing rates of individual neurons are certainly low-dimensional information. However, in order to accurately determine a firing rate, excessively long integration windows are required when the firing rate is low (Shadlen and Newsome 1998; Litvak et al. 2003). A new method for quantifying neuronal network dynamics is proposed in Rangan et al. (2008) by using a projection to event trees, which are statistical collections of spatial-temporal sequences of correlated network activities over coarse-grained times. When this event tree-based projection is applied to idealized integrate-and-fire (I&F) networks and a large scale realistic computational model (Cai et al. 2005; Rangan et al. 2005) of mammalian primary visual cortex (V1), it can effectively and efficiently capture essential stimulus-specific, and transient, variations in the full dynamics of neuronal networks. Therefore, we can use the information carried by the event trees for swift *discriminability*, i.e., the ability to discriminate fine input features over a short observation window T_{obs}. In addition, through the large set of diverse event trees, it is possible for them to be able to encode many distinct stimulus features simultaneously (note that n features constitute an n-dimensional space that characterizes the input), as is discussed within spike metric coding (Victor and Purpura 1997). The proof of concept for the event tree analysis is illustrated in Rangan et al. (2008) through the idealized I&F networks and the large scale V1 model indicates the possible application of event trees for extracting fine features coded in real cortices. This event chain analysis may potentially become a useful computational tool for analyzing experimental data.

We emphasize that in the event tree analysis, the entire event tree collectively serves as a signal within the network. Each individual spike of a particular neuron is merely a subcomponent of this signal. The information represented through event trees is a network-distributed or space-time-distributed signal, which is a function of both the network's architecture and its dynamic regime. Therefore, we can quantify this event tree signal statistically without restriction to any particular type of network architecture.

Networks of conductance-based I&F neurons have been used to simulate the dynamics and study the properties of large scale neuronal networks (Somers et al. 1995; Troyer et al. 1998; McLaughlin et al. 2000; Rangan and Cai 2007). Here, we consider a physiologically realistic Hodgkin-Huxley (HH) model, which accounts for the detailed generation of action potentials due to voltage-dependent membrane conductances arising from ionic channels (Hodgkin and Huxley 1952; Dayan and Abbott 2001). However, the complexity of the HH model precludes detailed analytical studies of its quantitative properties, hence one often resorts to numerical simulations to study them. In general, we cannot take large time steps to solve the HH neuron equations since they are stiff when the neuron is spiking. But in network simulations we often need to investigate the system's behavior for many different sets of parameters or to perform a statistical analysis over many trial conditions. It is therefore often necessary to integrate the dynamics with an efficient algorithm that allows us to use as large a time step as possible.

Inspired by the simplicity of the I&F model, we have proposed a specialized numerical method which reduces the dynamics of the HH neuron model to an I&F-like model (Sun et al. 2009). This method, referred to as the *library* method, can overcome the time step limitation due to the stiffness of the HH neuron model. During a single action potential, the ion currents cause the membrane potential to rise and drop down very rapidly and the HH dynamics is very stiff, for which we need a sufficiently small time step to resolve the dynamics numerically. The time interval of an action potential can last about 3 ms and the neuron cannot fire again during this period, i.e., in the absolute refractory period, which is explicitly imposed in the I&F model. Based on this observation, we take the following strategy. Once the membrane potential reaches the threshold value (say, -50mV), we stop evolving the HH neuron model and restart the integration after the refractory period with the reset values of the membrane potential and other gating variables. However, unlike in the I&F model for which the membrane potential is fixed to be the reset value during the refractory period, here in our method we can recover the time-courses of the membrane potential (as well as other dynamic gating variables) from a pre-computed high resolution data library. By this means we can circumvent numerical issues associated with stiffness, and use reasonably large time steps to evolve the HH neuron model.

In our previous work (Sun et al. 2009), by using several statistical measures, such as average firing rate and power spectrum analysis of voltage traces, we demonstrated that the numerical results using the library method with much larger time steps are consistent with those obtained by the standard method (say, Range-Kutta methods) with smaller time steps, and the long time low-order statistical results are in very good agreement between the library method and the standard method. We also examined whether fine dynamical bifurcation structures reflected in transient dynamics between the library method and the standard method could be different. As noted above, the coarse-grained event tree analysis is designed to discriminate the

difference between stimuli using statistical structures of event chains. Therefore, it is interesting to study whether simulation results obtained using the library method can be examined using this event tree analysis. In this work, we will further employ the event tree analysis to study whether the library method can produce HH network dynamics with higher order statistics preserved. Here we find that the event tree analysis is sensitive to high order structures in the dynamics simulated by both the standard and the library methods. We show that the library method is very efficient in the sense that the numerical results obtained using this method contain higher order event chains that are similar to the HH neuronal networks and that these event chains can be used in the event tree analysis for discrimination of fine input features. Combining the previous results (Sun et al. 2009), our results demonstrate that the library method may have a wide application in efficient numerical simulations of HH network dynamics arising from realistic settings.

The outline of the paper is as follows. In Section 2, we present a brief description of our HH neuronal network model and recapitulation of both the standard and the library methods for evolving the HH network dynamics. In Section 3, the coarse-grained event tree analysis is described and the discriminability function is constructed. In Section 4, we show numerical results of event tree analysis in three different dynamic regimes, which typically occur in the HH neuronal network dynamics. Then, we further compare the results of the standard and the library methods. These results well illustrate the advantage of our methods. Finally, we present conclusions in Section 5.

2 Methods

2.1 The network of Hodgkin-Huxley neurons

The dynamics of a Hodgkin-Huxley (HH) neuronal network with N neurons is governed by

$$C\frac{d}{dt}V_i = -G_{\mathrm{Na}}m_i^3h_i(V_i - V_{\mathrm{Na}}) - G_{\mathrm{K}}n_i^4(V_i - V_{\mathrm{K}}) - G_{\mathrm{L}}(V_i - V_{\mathrm{L}}) + I_i^{\mathrm{input}}, \tag{1}$$

$$\frac{dm_i}{dt} = \alpha_m(V_i)(1 - m_i) - \beta_m(V_i)m_i, \tag{2}$$

$$\frac{dh_i}{dt} = \alpha_h(V_i)(1 - h_i) - \beta_h(V_i)h_i, \tag{3}$$

$$\frac{dn_i}{dt} = \alpha_n(V_i)(1 - n_i) - \beta_n(V_i)n_i, \tag{4}$$

where the index i labels the neuron in the network, C is the cell membrane capacitance and V_i is its membrane potential, m_i and h_i are the activation and inactivation variables of the sodium current, respectively, and, n_i is the activation variable of the potassium current (Hodgkin and Huxley 1952; Dayan and Abbott 2001). The parameters G_{Na}, G_{K}, and G_{L} are the maximum conductances for the sodium, potassium and leak currents, respectively, V_{Na}, V_{K}, and V_{L} are the corresponding reversal potentials. Functional forms and parameters values for the HH neuron equations are given in Appendix A.

In our conductance-based network model, I_i^{input} stands for the synaptic input current, which is given by

$$I_i^{\mathrm{input}} = -\sum_{\mathrm{Q}} G_i^{\mathrm{Q}}(t)\left(V_i(t) - V_{\mathrm{G}}^{\mathrm{Q}}\right), \tag{5}$$

where $G_i^{\mathrm{Q}}(t)$ are the conductances with the index Q running over the types of conductances used, i.e., inhibitory and excitatory, and $V_{\mathrm{G}}^{\mathrm{Q}}$ are their corresponding reversal potentials (see Appendix A). The dynamics of $G_i^{\mathrm{Q}}(t)$ are governed by

$$\frac{d}{dt}G_i^{\mathrm{Q}}(t) = -\frac{G_i^{\mathrm{Q}}(t)}{\sigma_{\mathrm{r}}^{\mathrm{Q}}} + \widetilde{G}_i^{\mathrm{Q}}(t), \tag{6}$$

$$\frac{d}{dt}\widetilde{G}_i^{\mathrm{Q}}(t) = -\frac{\widetilde{G}_i^{\mathrm{Q}}(t)}{\sigma_{\mathrm{d}}^{\mathrm{Q}}} + \sum_{j\neq i}\sum_k \widetilde{S}_{i,j}^{\mathrm{Q}}\delta\left(t - T_{j,k}^{\mathrm{S}}\right) + \sum_k F_i^{\mathrm{Q}}\delta\left(t - T_{i,k}^{\mathrm{F}}\right). \tag{7}$$

Each neuron is either excitatory or inhibitory, as indicated by its type $\mathscr{L}_i \in \{\mathrm{E}, \mathrm{I}\}$. There are two conductance types $\mathrm{Q} \in \{\mathrm{E}, \mathrm{I}\}$ also labeling excitation and inhibition. We say an action potential or emission of a spike occurs at time t if the membrane potential of a neuron (say the jth neuron of type Q) reaches a threshold value V^{th} at that time. Then the spike triggers postsynaptic events in all the neurons that the jth neuron is presynaptically connected to and changes their Q-type conductances with the coupling strengths $\widetilde{S}_{i,j}^{\mathrm{Q}}$. On the other hand, for the postsynaptic ith neuron, its Q-type conductance $G_i^{\mathrm{Q}}(t)$ is determined by all spikes generated in the past from the presynaptic neurons of type Q. The term $\widetilde{G}_i^{\mathrm{Q}}(t)$ is an additional variable to describe the decay dynamics of conductance and the variable $G_i^{\mathrm{Q}}(t)$ has an impulse response with the form of an α-function with both a fast rise and a slow decay timescale, $\sigma_{\mathrm{r}}^{\mathrm{Q}}$ and $\sigma_{\mathrm{d}}^{\mathrm{Q}}$, respectively. The time $T_{j,k}^{\mathrm{S}}$ stands for the kth spike of neuron j prior to time t. The excitatory (inhibitory) conductance $\widetilde{G}^{\mathrm{E}}$ ($\widetilde{G}^{\mathrm{I}}$) of any neuron is increased when that neuron receives a spike from another excitatory

(inhibitory) neuron within the network. This is achieved as follows: The coupling strengths $\widetilde{S}^{\mathrm{E}}_{i,j}$ are zero whenever $\mathscr{L}_j = \mathrm{I}$, and similarly $\widetilde{S}^{\mathrm{I}}_{i,j}$ are zero whenever $\mathscr{L}_j = \mathrm{E}$. For the sake of simplicity, we consider an all-to-all heterogeneously coupled neuronal network, in which $\widetilde{S}^{\mathrm{Q}}_{i,j}$ is exponentially distributed (see Section 4.1 for the definition of $\widetilde{S}^{\mathrm{Q}}_{i,j}$). However, our method can readily be extended to more complicated networks that can encode many different types of network architecture.

The system is also driven by feedforward inputs. Here we consider stochastic inputs: we use a spike train sampled from a Poisson process with rate ω as the feedforward input. We denote $T^{\mathrm{F}}_{i,k}$ as the kth spike from the feedforward input to the ith neuron and it instantaneously increases that neuron's Q-type $\widetilde{G}^{\mathrm{Q}}_i(t)$ by magnitude F^{Q}_i. For simplicity, we also take F^{Q}_i to be a constant, F^{Q}, for Q-type conductance of all neurons in the network. The typical values or ranges of $\sigma^{\mathrm{Q}}_{\mathrm{r}}$, $\sigma^{\mathrm{Q}}_{\mathrm{d}}$, $\widetilde{S}^{\mathrm{Q}}$ and F^{Q} can be found in Appendix A. For the numerical results reported here, we set $V^{\mathrm{th}} = -50\mathrm{mV}$. The simulation results of the network dynamics are insensitive to slight adjustments of the V^{th} value as demonstrated in Sun et al. (2009).

2.2 Numerical scheme

For network modeling, we need a stable and accurate numerical method to evolve the HH neuron equations coupled with the dynamics of conductances (Eqs. (1)–(7)) for each neuron. Since individual neurons interact with each other through conductance changes associated with presynaptic spike times, it is also necessary to have numerical interpolation schemes that can determine the spike times accurately and efficiently (Hansel et al. 1998; Shelley and Tao 2001). In our numerical study, we use the Runge-Kutta fourth-order scheme (RK4) with fixed time step for integrating the system, along with a cubic Hermite interpolation for estimating spike times. The whole scheme is fourth-order accurate. In Appendix B, Algorithm 1 details this standard numerical scheme for a single neuron.

When simulating the network dynamics, we need to carefully take into account the causality of spiking events within a single time step via spike-spike interactions, especially for large time steps (Rangan and Cai 2007). Here, we choose a strategy similar to the event-driven approach (Mattia and Del Giudice 2000; Reutimann et al. 2003; Rudolph and Destexhe 2007). We take the spike-spike correction procedure, which is equivalent to stepping through the sequence of all the synaptic spikes within one time step and computing the effect of each spike on all future spikes. We step through this correction process until the neuronal trajectories and spike times of neurons converge. Details of this spike-spike correction algorithm and the general coupling strategy are discussed in Rangan and Cai (2007).

Although the standard numerical scheme with the spike-spike corrections can evolve the HH neuronal networks quite accurately, there is still some limitation on the time step. It is because explicit Runge-Kutta (RK) methods have finite domains of stability, and will have stability problems in solving Eq. (1) if the conductances are high (i.e., the HH neuron equations are stiff) and the time step Δt is large. Standard linearly stable schemes such as implicit Euler methods tend to be of low order accuracy when applied to smooth ODEs (Gear 1971), and may not be very accurate if Δt is large. Moreover, we also have three Eqs. (2) to (4) for the gating variables m, h, n coupled with Eq. (1) to be solved simultaneously, so an implicit method may not be efficient since it requires extra computation for solving the system iteratively in each step.

To overcome the time step limitation due to the stiffness, we proposed the library method (Sun et al. 2009), which treats the HH neuron like an I&F neuron. We briefly describe the idea of the method here. When the membrane potential $V(t)$ reaches a preset threshold value V^{th}, we stop evolving the HH neuron equations associated with this neuron since the total current (i.e., the right-hand side of Eq. (1)) becomes very large after this moment, making these equations very stiff. Instead of resolving the action potential by using a very small time step, we recover the action potential from our precomputed high resolution data library. Besides the potential $V(t)$, we also have the *intermediate replica*, i.e., the time courses of the gating variables m, h, n during the spiking period. The action potential takes a certain time duration like an absolute refractory period in the I&F model. At the end of this period, the potential $V(t)$ is hyperpolarized and the total current returns to a sufficiently small value. This allows us to evolve the HH neuron equations of this neuron using a large time step as before. Since the values of V, m, h, n at the end of this period are not fixed, depending on the strength of the input current, we need to build the data library in advance. The details of how to build the data library can be found in Sun et al. (2009). Here, we take the same high resolution data library as in our previous work. In Appendix C, Algorithm 2 details the library method for a single neuron.

The main advantage of our library method is that we can evolve the HH neuronal networks using a much larger time step than the one used for resolving the whole trajectories without the library, while achieving

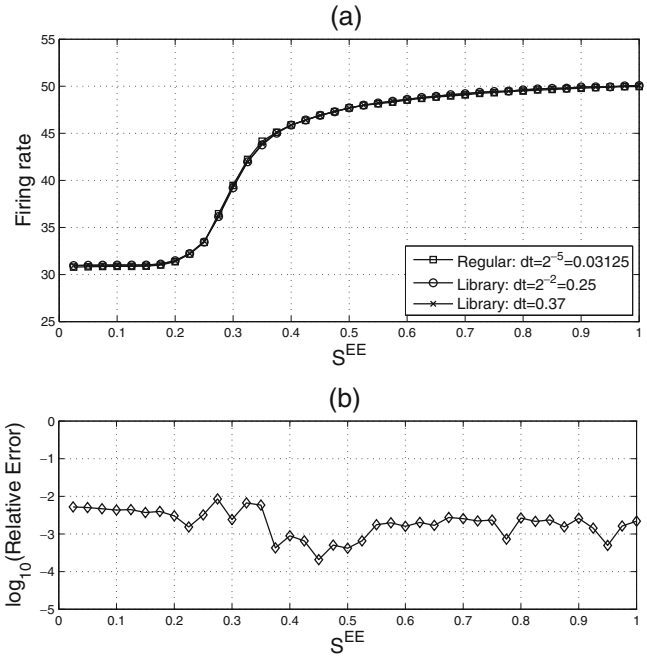

Fig. 1 The comparison results of an all-to-all heterogeneously connected network of 75 excitatory neurons and 25 inhibitory neurons driven by a feedforward input of a particular realization of a Poisson process with the rate $\omega = 50$ Hz (see Section 4.1 for more details). We fix the maximum values of the coupling strength for inhibitory (excitatory) synapses onto excitatory (inhibitory) neurons $S^{\mathrm{EI}} = S^{\mathrm{IE}} = 0.1$ mS/cm^2, the maximum value of recurrent inhibitory coupling strength $S^{\mathrm{II}} = 0.1$ mS/cm^2, and vary the maximum value of recurrent excitatory coupling strength S^{EE} ranging from 0.025 to 1.0 mS/cm^2. (**a**): Average firing rate versus the maximum coupling strength S^{EE}. The *squares* correspond to the result using the standard method with time step ($\Delta t = 0.03125$ ms); the *circles* represent the one computed with much larger time step ($\Delta t = 0.25$ ms) by using the library method, and the *crosses* are the solution computed for the maximum time step ($\Delta t = 0.37$ ms) with the library method. (**b**): The relative error in the average firing rate, $E^{\mathrm{R}} = |R^{\mathrm{standard}} - R^{\mathrm{library}}|/R^{\mathrm{standard}}$, between the library method on maximum time step ($\Delta t = 0.37$ ms) and the standard method on small time step ($\Delta t = 0.03125$ ms) versus S^{EE}. The total run time is 65536 ms

comparable numerical resolution in statistical quantifications. In Fig. 1, the numerical results show that we can still obtain at least 2 or 3 digits of accuracy in the average firing rate by using a time step about 10 times larger than the typical time step used by the standard RK methods. Note that the average firing rate is a low order statistical characterization of a voltage trajectory. Moreover, our library method has allowed us to take large time steps ($\Delta t = 0.37$ ms) and circumvent the stability requirement of standard RK methods (the maximum time step at which the method is still stable is $\Delta t = 0.08$ ms). We refer to Sun et al. (2009) for more comparison results, such as power spectra of voltage traces.

3 The event tree analysis

In this section we briefly review the idea of the event tree and show how it can be used to discriminate fine input features. More details about this method and its application to a large scale V1 model can be found in Rangan et al. (2008).

3.1 Definition of the event chain and the event tree

The notion of an event tree takes a projection of the system dynamics down to a set of event chains. To define event chains, we need the following notation: let σ_t^j denote a firing event of the jth neuron at time t (not discretized), and let σ_I^j denote any firing event of the jth neuron that occurs during the time interval I. Then, given a time scale τ, an m-event chain, denoted by $\{\sigma^{j_1} \to \sigma^{j_2} \to \ldots \to \sigma^{j_m}\}$ (spanning neurons $j_1, \ldots, j_m$, which need not be distinct), is defined to be any event $\sigma_t^{j_m}$ conditioned on (i.e., preceded by) the events $\sigma_{[t-\tau,t)}^{j_{m-1}}, \ldots, \sigma_{[t-(m-1)\tau,t-(m-2)\tau)}^{j_1}$. Here we only consider firing events as the relevant observables to construct the event chain, as motivated by the physiological fact that neurons only directly respond to spikes, with no response to the absence of spikes. Figure 2 schematically illustrate the idea of event chains.

Given an observation window T_{obs} of the system, one can record every m-event chain for all m up to some $m_{\max}$. Note that the number of observed one-event chains $\{\sigma^{j_1}\}$ corresponds to the total number of spikes of the j_1th neuron during T_{obs}; the number of observed two-event chains $\{\sigma^{j_1} \to \sigma^{j_2}\}$ corresponds to the total number of spikes of the j_2th neuron that occur within τ ms after a spike of the j_1th neuron; and so forth.

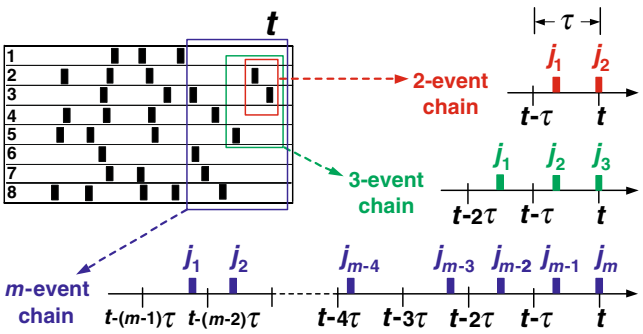

Fig. 2 Illustration of the event chains produced by a network of eight coupled neurons. The upper left in this figure is a raster plot for these eight neurons. An m-event chain, denoted by $\{\sigma^{j_1} \to \sigma^{j_2} \to \ldots \to \sigma^{j_m}\}$, is defined to be any event $\sigma_t^{j_m}$ conditioned on (i.e., preceded by) the events $\sigma_{[t-\tau,t)}^{j_{m-1}}$, $\sigma_{[t-2\tau,t-\tau)}^{j_{m-2}}$, $\ldots$, $\sigma_{[t-(m-1)\tau,t-(m-2)\tau)}^{j_1}$

We refer to the full collection of all possible $m \leq m_{\max}$ event chains with their occurrence counts as the $m_{\max}$-event tree over T_{obs}. An event tree can be thought of as an approximation to the set of conditional probabilities $P_{\tau}^{j_1,\ldots,j_m}$, i.e.,

$$P\left(\sigma_t^{j_m} | \sigma_{[t-\tau,t)}^{j_{m-1}}, \sigma_{[t-2\tau,t-\tau)}^{j_{m-2}}, \ldots, \sigma_{[t-(m-1)\tau,t-(m-2)\tau)}^{j_1}\right)$$

over the window T_{obs}. We remark that both the observation window size T_{obs} and the given time scale τ should be dictated by the dynamics being studied. In many cases, rich network properties can be revealed by choosing T_{obs} comparable to the system memory and τ comparable to the characteristic time scale over which one neuron can directly affect the dynamics of another through a synapse ($\tau \approx$ 2-20 ms). By keeping the τ-separation of events within each event chain, the event tree can contain more dynamic information than does a record of event orderings within the network (Thorpe and Gautrais 1998).

Figure 3 shows a schematic illustration of the event chains produced by a network of three coupled neurons. The system is driven by two slightly different stimuli I_1 and I_2. We record all pairs of events in which the second firing event occurs no later than τ ms after the first. Three such two-event chains, $\{\sigma^1 \to \sigma^2\}$, $\{\sigma^1 \to \sigma^3\}$, and $\{\sigma^2 \to \sigma^3\}$, are highlighted in Fig. 3(e). Note that the events $\sigma^1, \sigma^2, \sigma^3$ each occur two times within both rasters in Fig. 3(a) and (b). Figure 3(c) and (d) shows representations of the two-event tree corresponding to (a) and (b), respectively. Note that the event chain $\{\sigma^1 \to \sigma^3\}$ occurs twice within raster (b) but zero times within raster (a), whereas the event chain $\{\sigma^3 \to \sigma^1\}$ occurs zero times within raster (b) but twice within raster (a). The T_{obs} ms rasters in Fig. 3(a) and (b) clearly show that firing rate and oscillation frequency cannot be used to classify correctly the input underlying these typical T_{obs} ms observations of the system. However, due to different temporal ordering, it is clear that the two-event trees over these T_{obs} ms rasters can correctly classify the inputs. Figures 4 and 5 show the cases of a network of eight coupled neurons with $m_{\max} = 3$, where the numerical results obtained by using our library method also retain many dynamical features of the original system, and the occurrence rate of most event chains are similar to those produced by the standard method. This similarity shows that the library method can be used to evolve the HH neuronal network dynamics with high order statistics preserved. We will also discuss below whether the numerical results of the library method can be used in the event tree analysis of fine discrimination tasks.

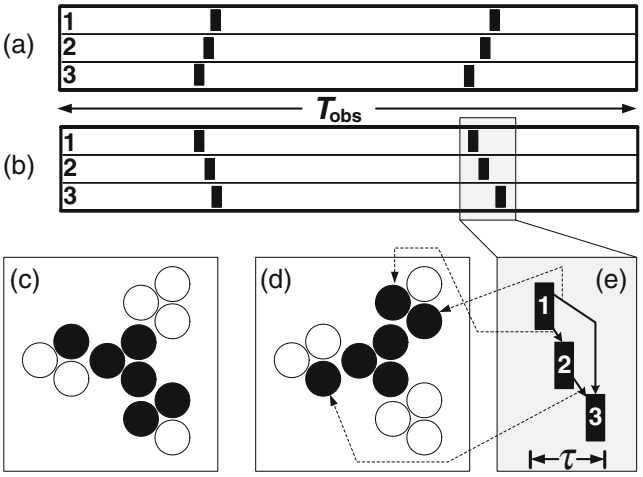

Fig. 3 Illustration of the event chains produced by a network of three coupled neurons. The system is driven by two slightly different stimuli, I_1 and I_2. The different colors stand (here only two colors, black and white), in general, for the number of occurrences over T_{obs} or "occurrence count" of the event $\sigma_t^{j_m}$ conditioned on $\sigma_{[t-\tau,t)}^{j_{m-1}}, \sigma_{[t-2\tau,t-\tau)}^{j_{m-2}}, \ldots, \sigma_{[t-(m-1)\tau,t-(m-2)\tau)}^{j_1}$. (**a**) The raster plot of the network under stimulus I_1 over T_{obs}. (**b**) Raster plot under stimulus I_2, with the same initial conditions as (**a**). (**c–d**) Representations of the two-event tree corresponding to (**a**) and (**b**), respectively. The singleton events $\{\sigma^j\}$ of the jth neuron are displayed within the central circles at complex vector location $e^{2\pi i(j-0.5)/3}$ with their occurrence count indicated by *black* (2 recorded events) or *white* (0 recorded events). The occurrence count of event pairs $\{\sigma^j \to \sigma^k\}$ are shown in the peripheral circles (displayed at complex vector location $3e^{2\pi i(j-0.5)/3} + e^{2\pi i(k-0.5)/3}$). (**e**) This panel zooms in on the second single synchronous burst observed in raster (**b**). The three black rectangles correspond to spikes, and the three two-chains, $\{\sigma^1 \to \sigma^2\}$, $\{\sigma^1 \to \sigma^3\}$, and $\{\sigma^2 \to \sigma^3\}$, each correspond to a different position within the graphic representation of (**d**), and these positions are indicated with dashed arrows leading from the event chains in raster plot (**e**) to their corresponding locations in the graphical representation (**d**)

3.2 Discriminability

The event tree described above is a natural intermediate projection of the system dynamics with a dimension $N^{m_{\max}}$. However, when N or $m_{\max}$ is large, there is a severe undersampling problem associated with analyzing the set of event trees produced by the network over multiple trials of a given T_{obs}. Namely, given multiple T_{obs} trials, each trial will in general produce a different event tree, and it is very difficult to estimate accurately the full joint probability distribution (over multiple trials) of the $\sim N^{m_{\max}}$ various event chains comprising the event trees. But we can circumvent this difficulty by considering first the probability distribution (over multiple trials of T_{obs} ms) of the observation count of each event chain individually and then considering the full collection of all these observation-distributions of

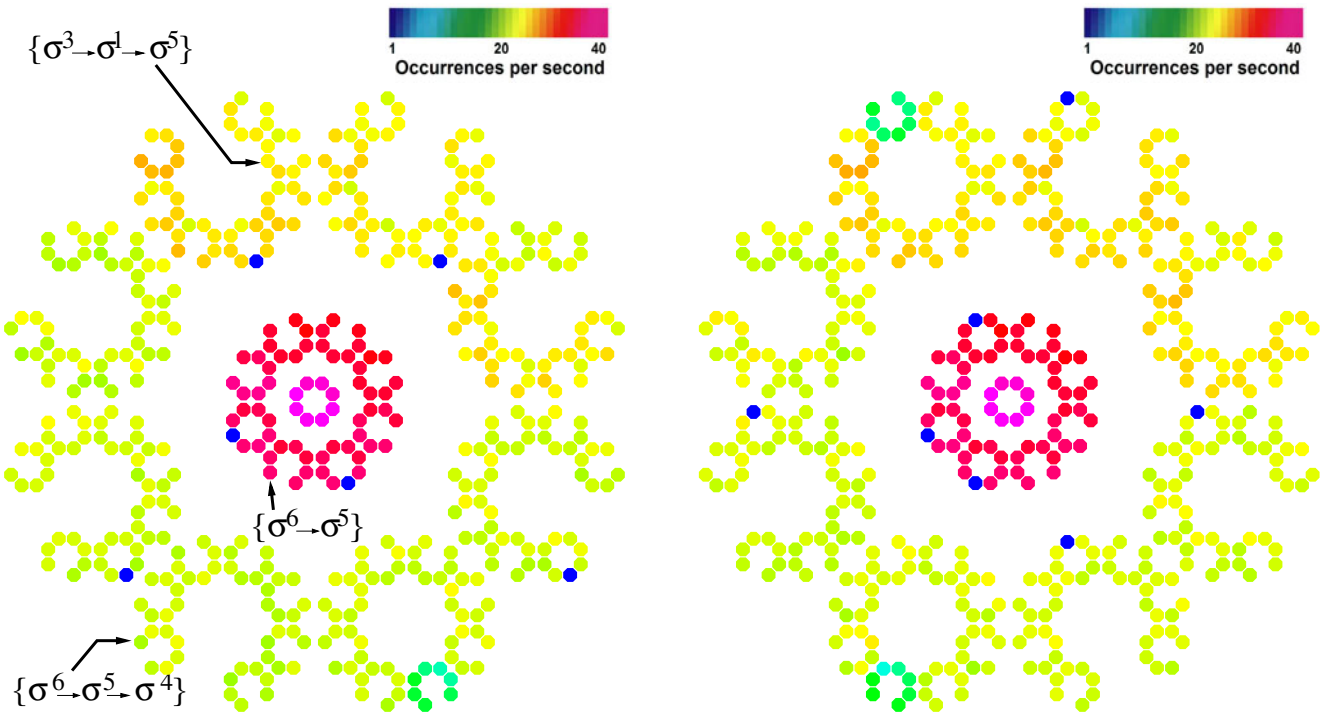

Fig. 4 The three-event trees collected over $T_{\text{obs}} = 512$ (with the coarse-grained time interval $\tau = 8$ ms) of the chaotic regime ($S^{\text{EE}} = 0.3$, see Section 4 for more details about the dynamic regimes) under stimulus I_1 (with input rate $\omega_1 = 50$ Hz and strengths $F_1^{\text{E}} = F_1^{\text{I}} = 0.05$ mS/cm^2). The tree on the *left* is collected from the raster data obtained by using the standard method with a time step ($\Delta t = 0.03125$ ms); the tree on the *right* is collected from the raster data computed with a much larger time step ($\Delta t = 0.25$ ms) by using the library method. The colors correspond to occurrence rate, plotted logarithmically from 1 occurrence per second to 40 occurrences per second. Event chains with an occurrence rate less than 1 occurrence per second have intentionally not been plotted. The tree is represented by a collection of rings (*circles*). On each ring, the discrete set of angles $\theta_j = 2\pi(j - 0.5)/N$, $(j = 1, \ldots, N)$ labels the N neurons. For succinct representation, we choose $N = 8$ neurons out of the network. For example, consider the three-event chain $\{\sigma^3 \to \sigma^1 \to \sigma^5\}$, indicated by the circle pointed by an arrow. This single circle lies within a hierarchical structure—a ring of rings of rings. Its location can be defined in terms of the following three angles: the angle of the outer major ring in which it lies (with the orientation angle θ_3, because the first event is σ^3), followed by the angle of the medium ring in which it lies (with the orientation angle θ_1, since the second event is σ^1), followed again by the angle of the smallest ring in which it lies (with the orientation angle θ_5, as the third event is σ^5). Thus, the color of this single circle corresponds to the occurrence rate of the 3-event chain $\{\sigma^3 \to \sigma^1 \to \sigma^5\}$. All of the three-event chains are organized this way within the outer major ring (for example, another three-event chain $\{\sigma^6 \to \sigma^5 \to \sigma^4\}$ is shown). All the two-event chains can be organized in a similar hierarchical structure—a ring of rings, which is the middle medium ring (for example, the two-event chain $\{\sigma^6 \to \sigma^5\}$ is shown). Finally, the single inner ring in the center of the diagram represents the set of one-event chains. Note that the color coding of the one-event chain merely labels the firing rates of each of the N neurons on the ring. It is important to note that there is a strong similarity between the left and right panels, indicating that the higher order statistics of rich event chains in terms of occurrence rate are captured by our library method

event chains, which we also refer to as an event tree. It is this object that we use to assess the discriminability of network dynamics, i.e., the ability to classify the stimulus based on a T_{obs} sample of the dynamics.

We note that event chains are appropriate for estimating the observation-distributions and assessing discriminability. Since many distinct event chains can occur simultaneously, there can be a large amount of distinct, stimulus-sensitive event chains spanning different neurons in the network even within short ($T_{\text{obs}} \sim$ 100 ms) observations of networks with low firing rates. Because event chains are not mutually exclusive, multiple event chains can occur during each T_{obs}, and we can collect accurate T_{obs}-observation-distributions (one for each event chain) with relatively few trials. As discussed previously (Rangan et al. 2008), it is this statistical feature that enables our event tree projection to characterize robustly, over short T_{obs}, the transient response and relevant dynamic features of a network. As will be discussed below, it can be seen that a neuronal network contains information for swift discriminability when that network can generate sufficiently rich, effectively multidimensional dynamics that reflect the salient features of the input.

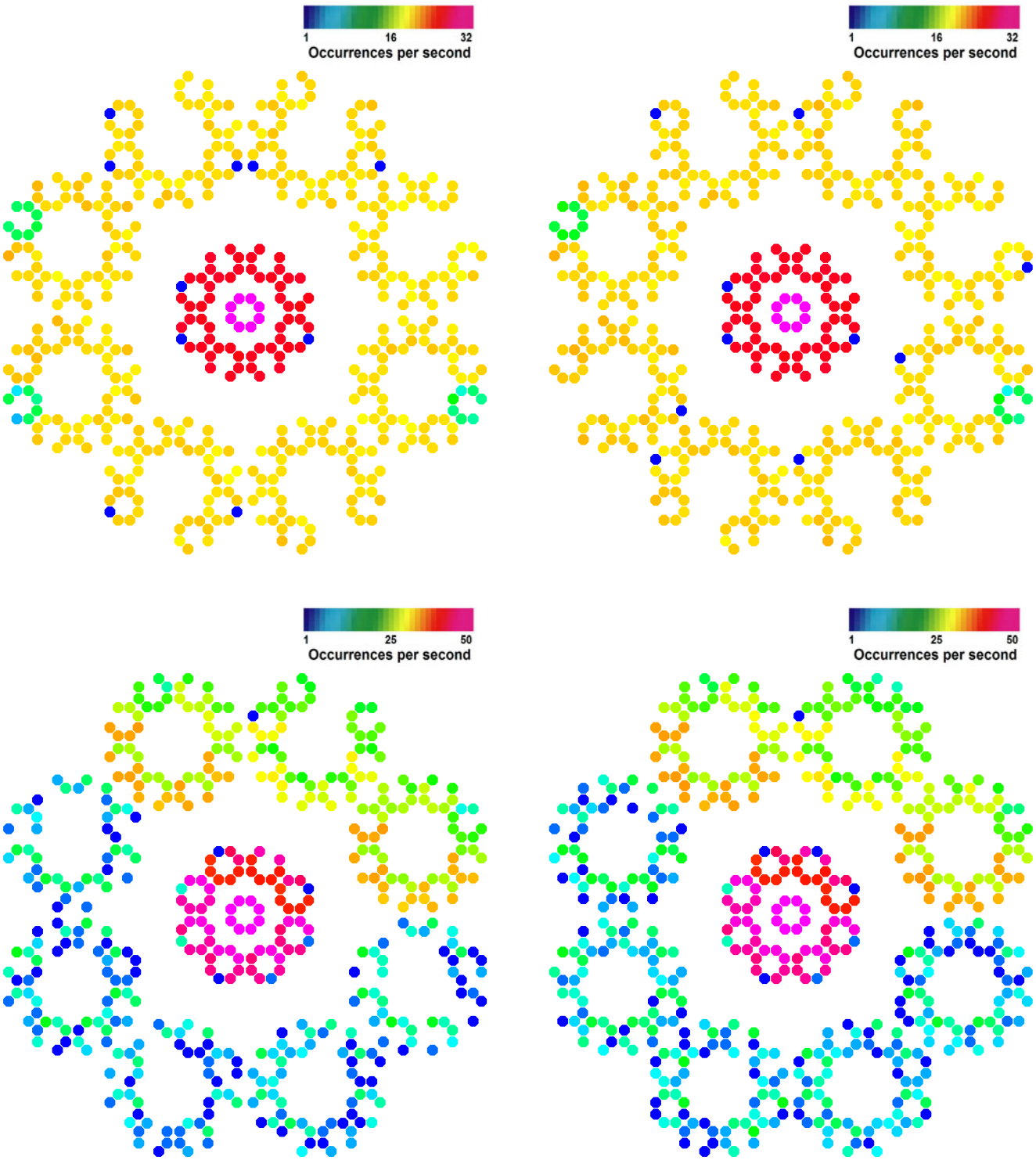

Fig. 5 The three-event trees collected over $T_{\text{obs}} = 512$ (with the coarse-grained time interval $\tau = 8$ ms) of the asynchronous regime ($S^{\text{EE}} = 0.1$, *top* panels) and the synchronous regime ($S^{\text{EE}} = 1.0$, *bottom* panels) under stimulus I_1 (with input rate $\omega_1 = 50$ Hz and strengths $F_1^{\text{E}} = F_1^{\text{I}} = 0.05$ mS/cm^2). The trees on the *left* are collected from the raster data obtained by using the standard method with a time step ($\Delta t = 0.03125$ ms); the trees on the *right* are collected from the raster data computed with a much larger time step ($\Delta t = 0.25$ ms) by using the library method. Note that for $S^{\text{EE}} = 0.1$ (*top* panels), the color scale for occurrence rate ranges from 1 occurrence per second to 32 occurrences per second; for $S^{\text{EE}} = 1.0$ (*bottom* panels), the color scale for occurrence rate ranges from 1 occurrence per second to 50 occurrences per second. Again note that there is a strong similarity between the left and right panels for these dynamical regimes, indicating that the higher order statistics of rich event chains in terms of occurrence rate are captured by our library method for all these dynamical regimes

Our discriminability function is constructed with standard methods from classification theory (Dayan and Abbott 2001), by assuming the observation counts of different event chains are independent. If the difference between the two empirical $T_{\rm obs}$ distributions under the stimuli I_1 and I_2 is significant, then the event-tree-projected network dynamics from a single $T_{\rm obs}$ observation can be used to discriminate between the stimuli. The procedure is as follows. More details can be found in Appendix D.

We say an event chain is not a good indicator of the stimulus if the $T_{\rm obs}$ distributions of occurrence counts of this event chain for I_1 and I_2 merge together. On the other hand, there are event chains that can be used to discriminate between the stimuli since the distributions corresponding of their occurrence counts to the two stimuli are fairly well separated. For instance, as depicted in Fig. 6, the $T_{\rm obs} = 512$ ms distribution of occurrence counts of the three-event chain $\{\sigma^3 \to \sigma^1 \to \sigma^5\}$ is quite different under stimulus I_1 than stimulus I_2. Therefore, the observation distribution of this event chain alone can be used to discriminate the inputs I_1 and I_2. For instance, we may take many independent single sample $T_{\rm obs} = 512$ ms observations of the network dynamics under different randomly chosen stimuli (either I_1 or I_2, with equal probability). For each of these samples, we obtain the occurrence count n of the $\{\sigma^3 \to \sigma^1 \to \sigma^5\}$ event chain, and determine a possible candidate stimulus by using these two distributions $P_1(\cdot)$ and $P_2(\cdot)$. We choose I_1 if $P_1(n) > P_2(n)$, otherwise we choose I_2 (e.g., in this case in Fig. 6, we guess I_2 if the event chain occurs eight or fewer times, otherwise we guess I_1). Applying this classification procedure to all different independent single samples can give us a probability of making a correct choice, i.e., a hit rate $A = \frac{1}{2}\sum_{n=0}^{\infty} \max\big(P_1(n), P_2(n)\big)$, and a false alarm rate $B = 1 - A$, and the information ratio $I_{I_1,I_2}^{\sigma^{j_1}\to\ldots\to\sigma^{j_m}} \equiv A/B$ (see Appendix D for more details). For this case in Fig. 6, we have $A = 79\%$, $B = 21\%$, and $I_{I_1,I_2}^{\sigma^3\to\sigma^1\to\sigma^5} \equiv A/B = 3.76$.

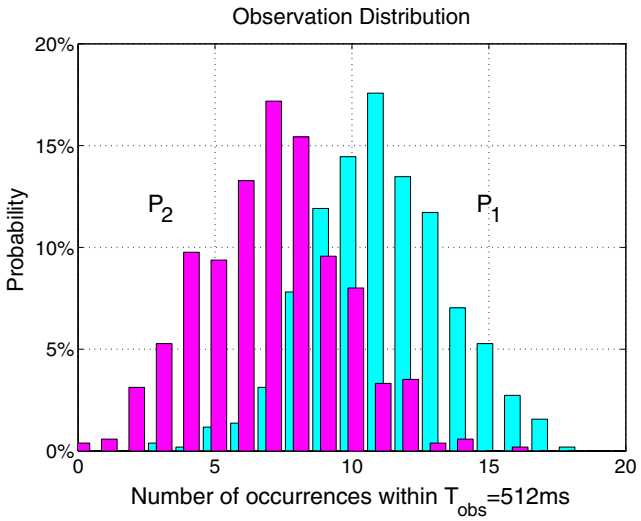

Fig. 6 The $T_{\rm obs} = 512$ ms distributions of occurrence counts of the three-event chain $\{\sigma^3 \to \sigma^1 \to \sigma^5\}$ with the *blue* and *pink* histograms, P_1 and P_2, corresponding to I_1 and I_2, respectively (I_1 with input rate $\omega_1 = 50$ Hz and input strengths $F_1^{\rm E} = F_1^{\rm I} = 0.05$ mS/cm^2; and I_2 with input rate $\omega_2 = 50$ Hz and input strengths $F_2^{\rm E} = F_2^{\rm I} = 0.0495$ mS/cm^2, i.e., there is a 1% difference in input strengths between two stimuli). The values of other parameters are the same as those in Fig. 4

The procedure described above classifies the stimulus underlying a single sample $T_{\rm obs}$ observation by considering only the occurrence count of a single event chain (i.e., a single element of the event tree). We can easily extend this procedure to incorporate every event chain within the event tree constructed from one $T_{\rm obs}$ observation. For example, given a sample $T_{\rm obs}$ observation and its associated event tree, we can independently use the occurrence count of each event chain within that event tree to estimate a possible candidate stimulus. Thus, each event chain "votes" for either stimulus I_1 or I_2, weighting each vote with the factor $\log\left(I_{I_1,I_2}^{\sigma^{j_1}\to\ldots\to\sigma^{j_m}}\right)$, which is a function of the information ratio of the contributing event chain. Then the weighted votes across the entire event tree are summed up to determine the candidate stimulus underlying the sample $T_{\rm obs}$ observation.

The discriminability of the $m_{\max}$-event tree (for this two-way discriminability task) is defined as the percentage of sample observations that were correctly classified under our voting procedure. For three-way discriminability tasks, we go through an analogous procedure, performing all three pairwise discriminability tasks for each sample observation and ultimately selecting the candidate stimulus corresponding to the majority. Note that the discriminability is a function of τ, $T_{\rm obs}$, and $m_{\max}$. As shown in the results in Figs. 10, 11, 12 and 13 in Section 4.2 below, for most of the systems we have observed, the discriminability increases as $m_{\max}$ and $T_{\rm obs}$ increase. More details can be found in Appendix D.

4 Results

4.1 Three dynamical regimes of the network

We consider an all-to-all heterogeneously connected HH network of 75 excitatory neurons and 25 inhibitory neurons driven by the feedforward input of a particular

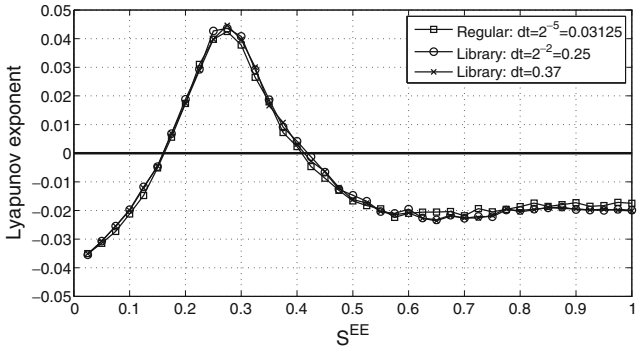

Fig. 7 The pseudo-Lyapunov exponent of the network of 75 excitatory and 25 inhibitory neurons with heterogeneous coupling strengths versus the maximum coupling strength parameter S^{EE} between the excitatory neurons. The network is driven by a feedforward input, which is a realization of a Poisson process with the rate $\omega = 50$ Hz. The total time of the trajectories is sufficiently long (65536 ms) in order to obtain statistically convergent results for the pseudo-Lyapunov exponent. As the same in Fig. 1, the *squares* correspond to the result using the standard method with time step ($\Delta t = 0.03125$ ms); the *circles* represent the one computed with much larger time step ($\Delta t = 0.25$ ms) by using the library method, and the *crosses* are the solution computed for the maximum time step ($\Delta t = 0.37$ ms) with the library method. The results here indicate our library method can achieve comparable resolution in the pseudo-Lyapunov exponent

realization of a Poisson process with the rate $\omega = 50$ Hz. We fix the maximum values of the coupling strength for inhibitory (excitatory) synapses onto excitatory (inhibitory) neurons $S^{\mathrm{EI}} = S^{\mathrm{IE}} = 0.1$ mS/cm^2, the maximum value of recurrent inhibitory coupling strength $S^{\mathrm{II}} = 0.1$ mS/cm^2, and vary the maximum value of the recurrent excitatory coupling strength S^{EE} ranging from 0.025 to 1.0 mS/cm^2 with an increment of $\Delta S^{\mathrm{EE}} = 0.025$ mS/cm^2. Other parameters are given in Appendix A. To make the connection heterogeneous, we generate an $N \times N$ random matrix $\mathbf{A}$ with exponentially distributed random elements $A_{i,j}$. Then the coupling strength for the jth neuron's synapses onto the ith neuron is given by $\widetilde{S}^{\mathrm{Q}}_{i,j} = \delta_{\mathrm{Q},\mathscr{L}_j} A_{i,j} S^{\mathscr{L}_i,\mathrm{Q}}/N^{\mathrm{Q}}$. Here, the Kronecker $\delta_{\mathrm{Q},\mathscr{L}_j}$ indicates that a spiking neuron can only increase the conductance associated with its type. The maximum coupling strength $S^{\mathscr{L}_i,\mathrm{Q}}$ only depends on the type of conductance Q, and the type of the postsynaptic neuron $\mathscr{L}_i$. The parameter N^{Q} is the total number of Q-type neurons in the network.

The systematic scanning result of the pseudo-Lyapunov exponents obtained by using our method (Sun et al. 2010) over a long time interval of $T = 2^{16} = 65536$ ms is shown in Fig. 7. As illustrated below, the result reveals three typical dynamical regimes—an asynchronous, a chaotic, and a synchronous regime. We refer to Sun et al. (2010) for the definition of the pseudo-Lyapunov exponents and the details of other quantifications that characterize these regimes, such as power spectrum analysis and numerical convergence tests.

(i) Asynchronous state For very small values of the maximum coupling strength S^{EE}, the drive to a single neuron due to the presynaptic spikes is so weak that the dynamics of each neuron is essentially driven by the feedforward input and the neurons fire at random, as is expected. The raster plot of the case $S^{\mathrm{EE}} = 0.1$ mS/cm^2 is shown in Fig. 8(a). This type of *asynchronous* states exists for $0.025 \lesssim S^{\mathrm{EE}} \lesssim 0.16$ mS/cm^2. In this regime, the firing times are reliable in the sense that they are not sensitive to numerical simulation time steps as long as they are sufficiently small (Sun et al. 2010).

This case is also characterized by the mean power spectrum, averaged over all neurons, of membrane

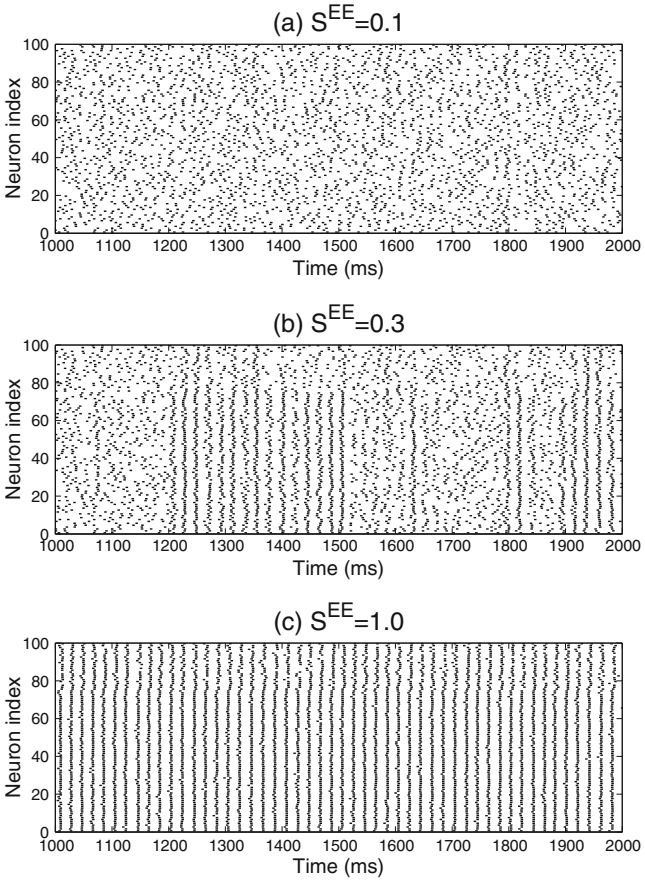

Fig. 8 Raster plots of spike events in the same network as the one in Fig. 7 computed with same initial conditions. The plots from (**a**) to (**c**) show typical cases of three dynamical regimes with the maximum coupling strength $S^{\mathrm{EE}} = 0.1$, 0.3, and 1.0 mS/cm^2, respectively: (**a**) Asynchronous dynamics; (**b**) Chaotic dynamics; (**c**) Synchronous dynamics. In each plot, the indices from 1 to 75 label the 75 excitatory neurons and the indices from 76 to 100 represent the other 25 inhibitory neurons in the network

potential trace (Fig. 9(a)). The power spectrum is of broad-band, with an asymptotic $\sim \omega^{-2}$ decay at high frequencies, signifying that (1) there are no clear oscillations in the dynamics, and (2) there is an exponential decay of time-correlations of the measured quantities, as implied by the Wiener-Khinchin theorem (Gardiner 1998).

(ii) Chaotic state For intermediate coupling strength, as shown in the raster plot of the case $S^{EE} = 0.3$ mS/cm^2 in Fig. 8(b), sometimes the neurons fire at random in an asynchronous way and sometimes they fire in an almost synchronous way, especially for the excitatory neurons. As indicated in Sun et al. (2010), the firing times seem to be unreliable and very sensitive to numerical time steps even if they are very small. Moreover, the statistical results for long time simulation show that the dynamics of the network is *chaotic* in the sense that the pseudo-Lyapunov exponent is measured to be positive, as shown in Fig. 7. The range for this type of states is $0.16 \lesssim S^{EE} \lesssim 0.41$ mS/cm^2.

The mean power spectrum, averaged over all neurons, of membrane potential trace in Fig. 9(b) also has a broad-band nature with small peaks. The power spectrum of this chaotic state is similar to that of the asynchronous state (Fig. 9(a)). However, there are weak peaks in the spectrum, typical of a chaotic dynamics, in which weak coherent synchronous oscillations coexist with irregular time dynamics (Schuster and Just 2005).

(iii) Nearly synchronous state When the coupling is strong, $S^{EE} \gtrsim 0.41$ mS/cm^2, a large portion of neurons in the network fire synchronously after a few of the neurons fire in advance. This firing pattern is shown in the raster plot in Fig. 8(c) for the case $S^{EE} = 1.0$ mS/cm^2. In this regime, firing times are again reliable as expected from the negative pseudo-Lyapunov exponent. (Sun et al. 2010).

As shown in Fig. 9(c), the mean power spectrum contains peaks clearly located at integer multiples of the fundamental frequency 50 Hz, indicating that the membrane potential evolves with a strong periodical component consistent with the feedforward input rate 50 Hz and the neurons fire almost synchronously, as seen in Fig. 8(c).

Figures 4 and 5 show the three-event trees collected from the raster data obtained by using the standard method and the library method, respectively, over $T_{obs} = 512$ (with the coarse-grained time interval $\tau = 8$ ms) of the three regimes. It is important to emphasize that there is a strong similarity between the left and right panels for these dynamical regimes, indicating that the higher order statistics of event chains (in terms of occurrence rate) are captured by our library method for all these dynamical regimes.

4.2 Discriminability in three dynamical regimes

As seen above, three different dynamical regimes contain rich high order statistical structures as characterized by the graphical representation of event chains and our library method can preserve these high order statistical structures well. Now we turn to the question of whether our library method can also produce statistically high order chains that encode inputs sensitively, and thus, can be revealed by our discriminability test. Here, we show the swift discriminability of the event

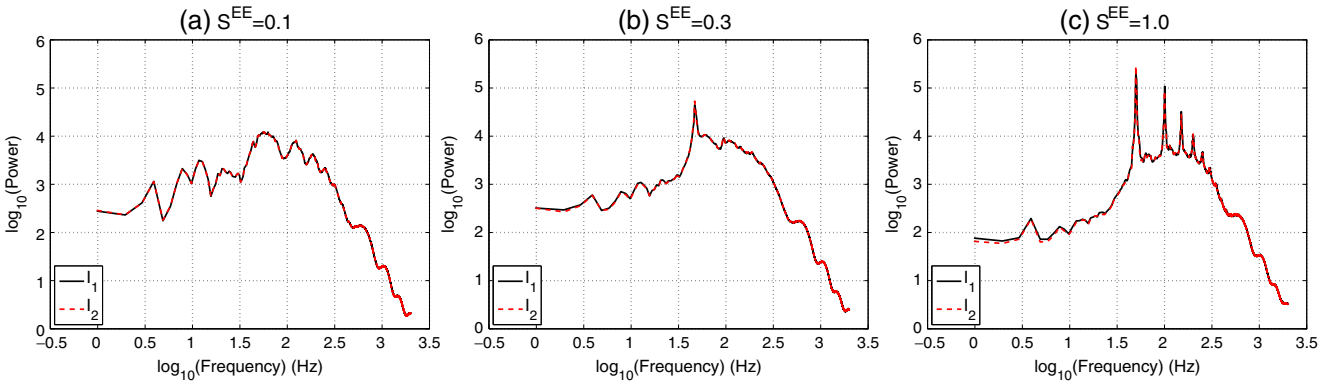

Fig. 9 The mean power spectrum, averaged over all neurons, of a neuron's membrane potential trace in the same network as the one in Fig. 7. The plots from (**a**) to (**c**) show three cases with the maximum coupling strength $S^{EE} = 0.1$, 0.3, and 1.0 mS/cm^2 corresponding to an asynchronous, chaotic and nearly synchronous regime, respectively. In each plot the *black (solid)* line corresponds to the power spectrum under the stimulus I_1; the *red (dashed)* line represents the power spectrum under the stimulus I_2. Note that these two curves essentially overlap with one another. As we used in Fig. 6, the stimuli I_1 and I_2 are very similar with only 1% difference in the input strength (for I_1: $\omega_1 = 50$ Hz and $F_1^E = F_1^I = 0.05$ mS/cm^2; and for I_2: $\omega_2 = 50$ Hz and $F_2^E = F_2^I = 0.0495$ mS/cm^2)

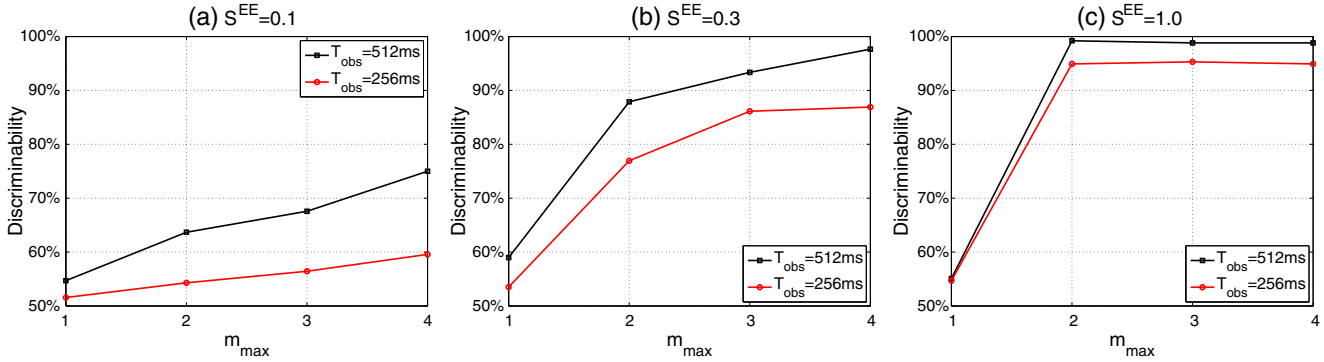

Fig. 10 Swift discriminability of the $m_{\max}$-event tree (with $\tau = 8$ ms) as a function of $m_{\max}$, with the ordinate denoting discrimination performance. As we used in Fig. 6, the stimuli I_1 and I_2 are very similar with only 1% difference in the input strength (for I_1: $\omega_1 = 50$ Hz and $F_1^{\mathrm{E}} = F_1^{\mathrm{I}} = 0.05$ mS/cm^2; and for I_2: $\omega_2 = 50$ Hz and $F_2^{\mathrm{E}} = F_2^{\mathrm{I}} = 0.0495$ mS/cm^2). The values of other parameters are the same as those in Fig. 7. The plots from (**a**) to (**c**) show three cases with the maximum coupling strength $S^{\mathrm{EE}} = 0.1$, 0.3, and 1.0 mS/cm^2 corresponding to an asynchronous, chaotic and nearly synchronous regime, respectively. In each plot the *black (squares)* line corresponds to the discriminability of the $T_{\mathrm{obs}} = 512$ ms observation; the *red (circles)* line represents the discriminability of the $T_{\mathrm{obs}} = 256$ ms observation

tree analysis for the network dynamics in each of three typical regimes, first, using the dynamics computed with the standard method, then, using the dynamics computed with the library method. For simplicity, from the network of total 100 neurons, we randomly choose $N = 8$ neurons to apply the event tree analysis. It seems that using a subset of different eight neurons or increasing the size of subset does not qualitatively change our conclusions on swift discriminability. The network is driven by independent Poisson stimuli I_1 and I_2 that are fully described by input rate ω_k and input strengths F_k^{E} and F_k^{I}, $(k = 1, 2)$. As with Fig. 6, the stimuli I_1 and I_2 are very similar (for I_1: $\omega_1 = 50$ Hz and $F_1^{\mathrm{E}} = F_1^{\mathrm{I}} = 0.05$ mS/cm^2; and for I_2: $\omega_2 = 50$ Hz and $F_2^{\mathrm{E}} = F_2^{\mathrm{I}} = 0.0495$ mS/cm^2), i.e., there is only 1% difference in the input strength between two stimuli. Here, we use the standard method with a small time step ($\Delta t = 0.03125$ ms) to evolve the network dynamics.

As shown in Fig. 9, within each dynamical regime, the power spectra under two stimuli strongly overlap each other. With these very similar inputs, the power spectra fail to discriminate the inputs within $T_{\mathrm{obs}} \leq 512$ ms. Figure 10 illustrates the utility of event tree analysis for swift discriminability. In all three dynamical regimes, the firing rate (i.e., $m_{\max} = 1$-event tree) cannot discriminate the stimuli very well. The discriminability of $T_{\mathrm{obs}} = 512$ ms event trees is higher than that of $T_{\mathrm{obs}} = 256$ ms event trees since an observation window of larger size can have more occurrence counts of event chains so that we may obtain more accurate statistics. We also note that the discriminability increases as $m_{\max}$ increases.

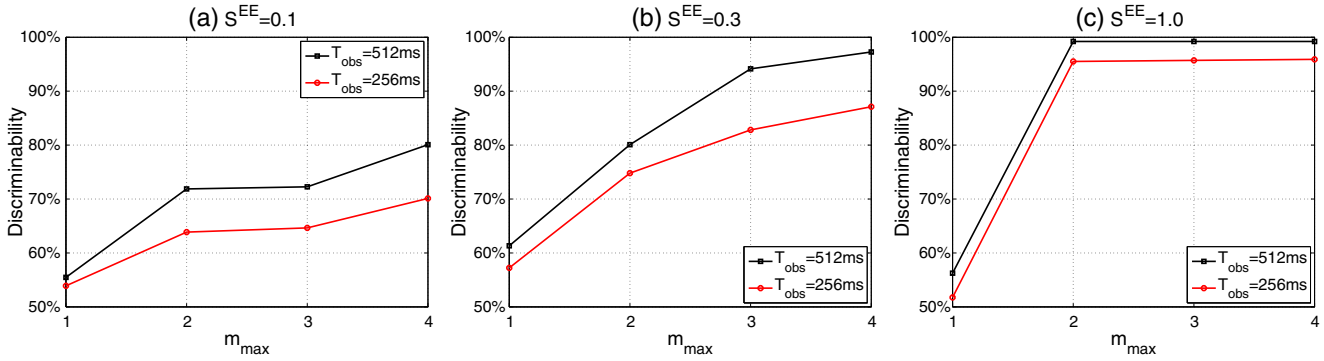

Fig. 11 Swift discriminability of the $m_{\max}$-event tree (with $\tau = 8$ ms) as a function of $m_{\max}$. The stimuli I_1 and I_2 are very similar with only 1% difference in the input rate instead of strength as in Fig. 10 (for I_1: $\omega_1 = 50$ Hz and $F_1^{\mathrm{E}} = F_1^{\mathrm{I}} = 0.05$ mS/cm^2; and for I_2: $\omega_2 = 49.5$ Hz and $F_2^{\mathrm{E}} = F_2^{\mathrm{I}} = 0.05$ mS/cm^2). The values of other parameters and the notations are the same as those in Fig. 10

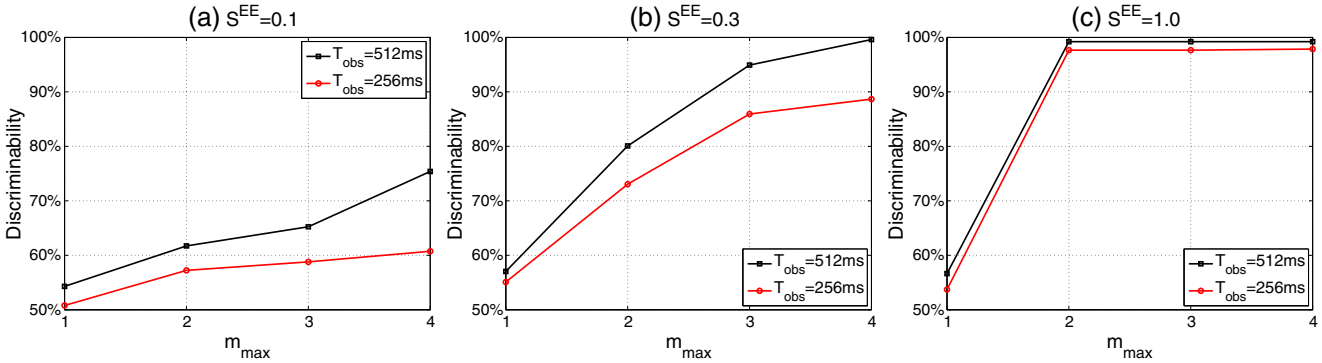

Fig. 12 Swift discriminability of the $m_{\max}$-event tree (with $\tau =$ 8 ms) as a function of $m_{\max}$ between the stimuli I_1 and I_2 with only 1% difference in the input strength. All the values of parameters and the notations are the same as those in Fig. 10, except that we use the library method with the large time step ($\Delta t = 0.25$ ms) to evolve the network dynamics

As shown in Fig. 10(a) of the asynchronous regime, all of $T_{\text{obs}} = 256$ ms event trees again cannot differentiate the stimuli very well, whereas only the deeper event tree ($m_{\max} = 4$) with $T_{\text{obs}} = 512$ ms can be used to classify correctly the stimulus $\sim 75\%$ of the time. In the chaotic regime shown in Fig. 10(b), both of the $T_{\text{obs}} = 256$ ms and $T_{\text{obs}} = 512$ ms event trees with $m_{\max} \geq 2$ can reliably discriminate I_1 and I_2 more than $\sim 78\%$ of the time. Figure 10(c) illustrates the discriminability in the nearly synchronous case, where the event trees with $m_{\max} \geq 2$ can discriminate very robustly between the stimuli more than $\sim 95\%$ of the time.

We also perform the swift discriminability of the event tree analysis by using another set of very similar stimuli I_1 and I_2, which now have only 1% difference in the input rate instead of strength (for I_1: $\omega_1 =$ 50 Hz and $F_1^{\text{E}} = F_1^{\text{I}} = 0.05$ mS/cm^2; and for I_2: $\omega_2 =$ 49.5 Hz and $F_2^{\text{E}} = F_2^{\text{I}} = 0.05$ mS/cm^2). Figure 11 shows the similar observations as Fig. 10 does, e.g., (i) the discriminability increases as $m_{\max}$ and T_{obs} increase; (ii) the network dynamics in the chaotic and nearly synchronous regimes is sufficiently rich that the event trees observed over a short $T_{\text{obs}} = 256$ ms can reliably encode small differences in the stimulus.

Now we turn to the discussion of the swift discriminability of the event tree analysis for the network dynamics evolved by using the library method. First, we repeat the test of the discriminability between two stimuli I_1 and I_2 that have only 1% difference in the input strength, as the one used in Fig. 10. But the network dynamics under both stimuli is evolved by using the library method with the large time step ($\Delta t = 0.25$ ms). As shown in Fig. 12, we obtain similar results as in Fig. 10.

Second, we repeat a test of the discriminability between two stimuli I_1 and I_2 that have only 1%

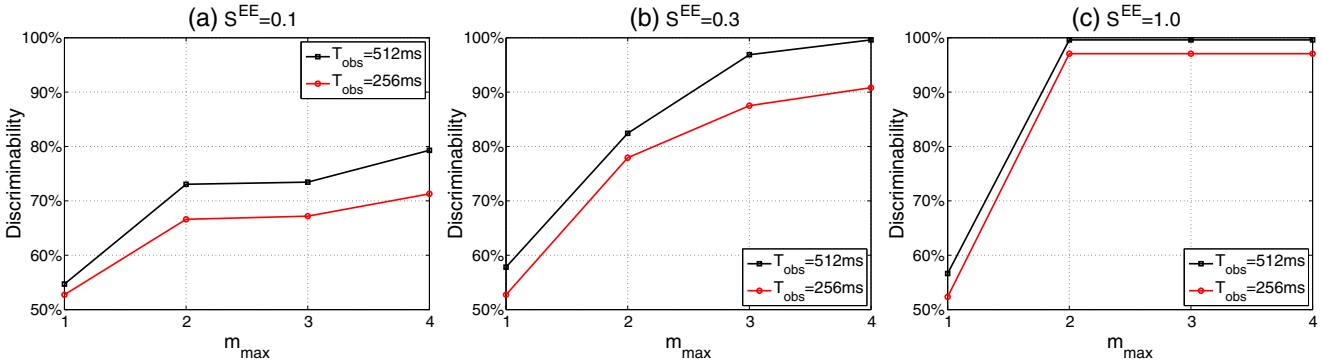

Fig. 13 Swift discriminability of the $m_{\max}$-event tree (with $\tau =$ 8 ms) as a function of $m_{\max}$ between the stimuli I_1 and I_2 with only 1% difference in the input rate. All the values of parameters and the notations are the same as those in Fig. 11, except that we use the library method with the large time step ($\Delta t = 0.25$ ms) to evolve the network dynamics

difference in the input rate, as the one used in Fig. 11. Once again, the network dynamics under both stimuli is evolved by using the library method with the large time step ($\Delta t = 0.25$ ms). Figure 13 shows similar results as in Fig. 11.

These tests indicate that we can employ the library method to simulate the HH neuronal networks using a much larger time step than the one used for resolving the whole trajectories without the library, while still producing stimulus-sensitive event chains. Therefore, our library method has the potential to be an efficient numerical method for simulating large neuronal network systems, even when high order statistical structures are needed.

5 Conclusion

We have presented a comparison between our library method and a standard high-resolution numerical method for evolving a set of HH neuronal networks. Specifically, we have compared a high-order statistical measurement of these systems' dynamics encapsulated by event chains and event trees. We have found that, not only does our library method serve to efficiently evolve the HH system, but our library method also captures many low- and high-order statistics of the network's dynamics. It has been demonstrated that these event chains and trees can potentially extract, with high reliability, the information that simultaneously encodes various stimuli within realistic short observation times. The event tree analysis does not rely on specific architectural assumptions and is applicable to both feedforward and strongly recurrent networks. Moreover, we have shown that event trees of a network can reliably capture relevant statistical information even when the network dynamics is chaotic. It is important to emphasize that the analysis of network dynamics using information represented in event trees can be extended to investigate much larger, more realistic neuronal systems, such as the primary visual cortex (V1) and provide discriminability of fine orientations within the V1 model (Rangan et al. 2008). An idea similar to event tree analysis has also been applied for discriminating different odors within a large-scale model of the fly antennal lobe. We expect that our computational methods for collecting, storing, and analyzing event trees can be used by experimentalists to study network mechanisms underlying biological functions by probing the relevance and stimulus specificity of diverse subsets of events within real networks through methods such as multielectrode grids.

The numerical study of the network dynamics of HH neurons in previous sections reveals three typical dynamical regimes—asynchronous, chaotic and synchronous—ones as the synaptic coupling strength varies from weak to strong. The regimes are characterized by several tools from dynamical systems theory, such as measuring the largest Lyapunov exponent and analyzing the power spectrum of voltage traces. Discriminability relies, particularly for fine discrimination tasks, on the network operating with sufficiently rich dynamics. As we have demonstrated, for the asynchronous regime, both power spectra and low order event trees cannot discriminate between fine stimulus characteristics with short observation windows. However, in the chaotic and nearly synchronous regimes, the event trees contain sufficient information that can reveal (over short observation windows) small differences between the stimuli which cannot be easily obtained by analyzing the power spectrum of oscillations. We emphasize that the event tree analysis indeed is a sensitive tool to differentiate high order statistics.

In this work, we further demonstrate that our library-based HH neuronal dynamics solver is an efficient numerical method for evolving the HH network dynamics. It numerically reduces the dynamics of HH neurons to that of I&F-like neurons by using a pre-computed high resolution data library. This method can overcome the stability restriction associated with firing events and allows us to use much larger time steps to evolve the neuronal trajectories even if the conductances are high and the HH equations are stiff. We emphasize that the library method can be practicable for simulating large-scale neuronal networks by incorporating a clustering procedure of firing events in networks to take advantage of localized architectures, such as spatial scales of strong local interactions, which are often present in large-scale computational models—for example, those of the V1. By using this method, we can collect accurate statistical information with much lower computational cost. Moreover, the numerical results obtained by using the library method retain sufficient high order statistics of firing events, which can also be used in the fine discrimination tasks with the event tree analysis.

Acknowledgements The work was supported by NSF grants DMS-0506396, DMS-0507901, DMS-1009575 and a grant from the Swartz foundation. Y. Sun was supported by NSF Joint Institutes' Postdoctoral Fellowship through SAMSI. D. Zhou was supported by Shanghai Pujiang Program (Grant No. 10PJ1406300) and NSFC (Grant No. 11026052). We thank two anonymous referees for helpful comments on the manuscript.

Appendix A: Parameter values for the Hodgkin-Huxley equations

Parameter values or ranges and function definitions of the Hodgkin-Huxley model are as follows (Dayan and Abbott 2001):

$$G_{\mathrm{Na}} = 120\ \mathrm{mS/cm^2},\quad V_{\mathrm{Na}} = 50\ \mathrm{mV},$$

$$G_{\mathrm{K}} = 36\ \mathrm{mS/cm^2},\quad V_{\mathrm{K}} = -77\ \mathrm{mV},$$

$$G_{\mathrm{L}} = 0.3\ \mathrm{mS/cm^2},\quad V_{\mathrm{L}} = -54.387\ \mathrm{mV},$$

$$C = 1\ \mu\mathrm{F/cm^2},\quad V_{\mathrm{G}}^{\mathrm{E}} = 0\ \mathrm{mV},\quad V_{\mathrm{G}}^{\mathrm{I}} = -80\ \mathrm{mV},$$

$$F^{\mathrm{E}} = 0.05 \sim 0.1\ \mathrm{mS/cm^2},\quad \widetilde{S}^{\mathrm{E}} = 0.05 \sim 1.0\ \mathrm{mS/cm^2},$$

$$F^{\mathrm{I}} = 0.01 \sim 0.05\ \mathrm{mS/cm^2},\quad \widetilde{S}^{\mathrm{I}} = 0.05 \sim 1.0\ \mathrm{mS/cm^2},$$

$$\sigma_{\mathrm{r}}^{\mathrm{E}} = 0.5\ \mathrm{ms},\quad \sigma_{\mathrm{d}}^{\mathrm{E}} = 3.0\ \mathrm{ms},$$

$$\sigma_{\mathrm{r}}^{\mathrm{I}} = 0.5\ \mathrm{ms},\quad \sigma_{\mathrm{d}}^{\mathrm{I}} = 7.0\ \mathrm{ms},$$

$$\alpha_m(V) = 0.1(V+40)/(1-\exp(-(V+40)/10)),$$

$$\beta_m(V) = 4\exp(-(V+65)/18),$$

$$\alpha_h(V) = 0.07\exp(-(V+65)/20),$$

$$\beta_h(V) = 1/(1+\exp(-(35+V)/10)),$$

$$\alpha_n(V) = 0.01(V+55)/(1-\exp(-(V+55)/10)),$$

$$\beta_n(V) = 0.125\exp(-(V+65)/80).$$

Appendix B: Numerical method for a single neuron

Here we provide details of the numerical method for evolving the dynamics of a single neuron. For simplicity, we use vector X_i to represent all the variables in the solution of the ith neuron:

$$X_i(t) = \big(V_i(t), m_i(t), h_i(t), n_i(t), G_i^{\mathrm{Q}}(t), \widetilde{G}_i^{\mathrm{Q}}(t)\big).$$

Given an initial time t_0 and time step Δt, initial values $X_i(t_0)$, and spike times $T_{i,k}^{\mathrm{F}}$ and $T_{j\neq i,k}^{\mathrm{S}}$ from the other neurons in the network, a preset threshold value V^{th} at which an action potential starts, our method computes a numerical solution of all variables $X_i(t_0+\Delta t)$ as well as the intervening spike times $T_{i,k}^{\mathrm{S}}$ (if any occurred) for the ith neuron as follows:

Algorithm 1. *(Single neuron scheme)*

Step 1: Input: an initial time t_0, a time step Δt, a set of spike times $T_{i,k}^{\mathrm{F}}$ and $T_{j\neq i,k}^{\mathrm{S}}$ and associated strengths F_i^{Q} and $\widetilde{S}_{i,j}^{\mathrm{Q}}$.

Step 2: Consider the time interval $[t_0, t_0+\Delta t]$. Let M denote the total number of feedforward and presynaptic spikes within this interval. Sort these spikes into an increasing list of M spike times T_m^{sorted} with corresponding spike strengths $S_m^{\mathrm{sorted,Q}}$. In addition, we extend this notation such that $T_0^{\mathrm{sorted}} := t_0$, $T_{M+1}^{\mathrm{sorted}} := t_0+\Delta t$ and $S_0^{\mathrm{sorted,Q}} = S_{M+1}^{\mathrm{sorted,Q}} := 0$.

Step 3: For $m = 1,\ldots,M+1$, advance the equations for the HH neuron model and its conductances (Eqs. (1)–(7)) from $T_{m-1}^{\mathrm{sorted}}$ to T_m^{sorted} using the standard RK4 scheme to obtain $X_i(T_m^{\mathrm{sorted}})$; Then, update the conductance $\widetilde{G}_i^{\mathrm{Q}}(T_m^{\mathrm{sorted}})$ by adding the appropriate strengths $S_m^{\mathrm{sorted,Q}}$.

Step 4: If the calculated values for $V_i(T_m^{\mathrm{sorted}})$ are each less than V^{th}, then we can accept $X_i(T_{M+1}^{\mathrm{sorted}})$ as the solution $X_i(t_0+\Delta t)$. We update $t_0 \leftarrow t_0+\Delta t$ and return to step 2 and continue.

Step 5: Otherwise, let $V_i(T_m^{\mathrm{sorted}})$ be the first calculated voltage greater than V^{th}. We know that the ith neuron fired somewhere during the interval $[T_{m-1}^{\mathrm{sorted}}, T_m^{\mathrm{sorted}}]$.

Step 6: In this case we use a high-order polynomial interpolation to find an approximation of the spike time t^{fire} in the interval $[T_{m-1}^{\mathrm{sorted}}, T_m^{\mathrm{sorted}}]$. For example, we can use the numerical values of $V_i(T_{m-1}^{\mathrm{sorted}})$, $V_i(T_m^{\mathrm{sorted}})$, $\frac{d}{dt}V_i(T_{m-1}^{\mathrm{sorted}})$, $\frac{d}{dt}V_i(T_m^{\mathrm{sorted}})$ to form a cubic polynomial. We record t^{fire} as the $(k+1)$th postsynaptic spike time $T_{i,k+1}^{\mathrm{S}}$ of the ith neuron. We update $t_0 \leftarrow t_0+\Delta t$ and return to step 2 and continue.

Appendix C: The library-based numerical method

Here, we briefly outline Algorithm 2, which uses the library to recover the spike. Given an initial time t_0 and time step Δt, initial values $X_i(t_0)$, and spike times $T_{i,k}^{\mathrm{F}}$ and $T_{j\neq i,k}^{\mathrm{S}}$ from the other neurons in the network, our method calculates a numerical solution of all variables $X_i(t_0+\Delta t)$ as well as the intervening spike times $T_{i,k}^{\mathrm{S}}$ (if any occurred) for the ith neuron as follows.

In order to build the data library, we choose N_{I} different values of I^{input} equally distributed in its range from 7.5 to 50.0 $\mu\mathrm{A/cm^2}$, which can essentially cover all typical values of I^{input} of the spiking neurons *at the moments when they fire* in our network simulations. We also equally distribute N_{lib} points of $m^{\mathrm{input}}, h^{\mathrm{input}}, n^{\mathrm{input}}$ in their parameter ranges, respectively. These ranges should cover all typical values of m, h, n of a neuron when it fires in the HH network.

Algorithm 2. *(Library algorithm)*

Step 0: Pre-compute the data library of V, m, h, n for N_{I} different values of the constant input current I^{input} using very fine time step δt. For each I^{input}, we

isolate an action potential form that starts exactly from $V^{\rm th}$ to a later time (after $T^{\rm ref}$ ms) where the membrane potential drops down around its minimum. Then we use this action potential form (i.e., the intermediate replica of the membrane potential) with different values of $m^{\rm input}$, $h^{\rm input}$, $n^{\rm input}$ as initial values to compute the intermediate replica for m, h, n individually. In particular, we can obtain the reset values $m^{\rm re}$, $h^{\rm re}$, $n^{\rm re}$ at the end point where the form of the action potential terminates. For each case of $I^{\rm input}$, there are $N_{\rm lib}$ data sets of m, h, n, respectively.

Step 1: Input: the library, an initial time t_0, a large time step Δt, a set of spike times $T^{\rm F}_{i,k}$ and $T^{\rm S}_{j\neq i,k}$ and associated strengths $F^{\rm Q}_i$ and $\widetilde{S}^{\rm Q}_{i,j}$.

Step 2: Consider the time interval $[t_0, t_0+\Delta t]$. Let M denote the total number of feedforward and presynaptic spikes within this interval. Sort these spikes into an increasing list of M spike times $T^{\rm sorted}_m$ with corresponding spike strengths $S^{\rm sorted,Q}_m$. In addition, we extend this notation such that $T^{\rm sorted}_0 := t_0$, $T^{\rm sorted}_{M+1} := t_0+\Delta t$ and $S^{\rm sorted,Q}_0 = S^{\rm sorted,Q}_{M+1} := 0$.

Step 3: For $m = 1, \ldots, M+1$, advance the equations for the HH neuron model and its conductances (Eqs. (1)–(7)) from $T^{\rm sorted}_{m-1}$ to $T^{\rm sorted}_m$ using the standard RK4 scheme to obtain $X_i(T^{\rm sorted}_m)$; Then, update the conductance $\widetilde{G}^{\rm Q}_i(T^{\rm sorted}_m)$ by adding the appropriate strengths $S^{\rm sorted,Q}_m$.

Step 4: If the calculated values for $V_i(T^{\rm sorted}_m)$ are each less than $V^{\rm th}$, then we can accept $X_i(T^{\rm sorted}_{M+1})$ as the solution $X_i(t_0+\Delta t)$. We update $t_0 \leftarrow t_0+\Delta t$ and return to step 2 and continue.

Step 5: Otherwise, let $V_i(T^{\rm sorted}_m)$ be the first calculated voltage greater than $V^{\rm th}$. We know that the ith neuron fired somewhere during the interval $[T^{\rm sorted}_{m-1}, T^{\rm sorted}_m]$.

Step 6: In this case we use a high-order polynomial interpolation to find an approximation to the spike time $t^{\rm fire}$ in the interval $[T^{\rm sorted}_{m-1}, T^{\rm sorted}_m]$. For example, we can use the numerical values of $V_i(T^{\rm sorted}_{m-1})$, $V_i(T^{\rm sorted}_m)$, $\frac{d}{dt}V_i(T^{\rm sorted}_{m-1})$, $\frac{d}{dt}V_i(T^{\rm sorted}_m)$ to form a cubic polynomial. We record $t^{\rm fire}$ as the $(k+1)$th postsynaptic spike time $T^{\rm S}_{i,k+1}$ of the ith neuron.

Step 7: We compute the values of $I^{\rm th} = -\sum_{\rm Q} G^{\rm Q}_i(t^{\rm fire})\times (V^{\rm th}-V^{\rm Q}_{\rm G})$, as well as the gating variables $m^{\rm th}$, $h^{\rm th}$ and $n^{\rm th}$ at this time. Then, we perform a linear interpolation to find the corresponding reset values of $V^{\rm re}, m^{\rm re}, h^{\rm re}, n^{\rm re}$ in the library. Meanwhile, we stop evolving Eqs. (1)–(5) for the next $T^{\rm ref}$ ms, but evolve Eqs. (6) and (7) for the conductance terms $G^{\rm Q}_i(t)$ and $\widetilde{G}^{\rm Q}_i(t)$ as usual. We update $t_0 \leftarrow \min(t^{\rm fire}+T^{\rm ref}, t+\Delta t)$ and return to step 2 and continue with the reset values $V^{\rm re}, m^{\rm re}, h^{\rm re}, n^{\rm re}$ as the initial values $V_i(t_0)$, $m_i(t_0)$, $h_i(t_0)$ and $n_i(t_0)$.

Appendix D: More details on discriminability

Here we provide details of several definitions we used in Section 3.2. Although the occurrence count rate n takes only discrete values as shown in the x-axis of Fig. 6, it is more convenient to treat n as a continuous variable for the following discussion. Given a single sample $T_{\rm obs}$ observation of the network dynamics, our discrimination task is to determine a possible candidate stimulus by using the two distributions $P_1(n)$ and $P_2(n)$ of an event chain. A simple procedure is to obtain the occurrence rate n of the event chain in the sample observation and compare it to a threshold number z. If $n > z$, we report I_1; otherwise we report I_2. Figure 6 shows that if we choose z to lie somewhere between the two distributions, say, the location where $P_1(z) = P_2(z)$, this procedure can give the correct answer when the two distributions are fairly well separated, but will have difficulty discriminating the stimuli if their distributions merge together. This difficulty is clearly related to the degree to which the two distributions overlap.

First, we show how to define and calculate the hit rate A. The probability that the procedure will make the correct choice (called a hit) under the stimulus I_1 is the conditional probability that $n > z$ given the stimulus I_1 was presented, $\alpha := P(n > z|I_1) = \int_z^\infty P_1(n)dn$. The probability that it will give the answer I_1 when the stimulus was actually I_2 (called a false alarm) is similarly $\beta := P(n > z|I_2) = \int_z^\infty P_2(n)dn$. These two probabilities completely determine the performance of the discrimination procedure because the probabilities for the other two cases (choosing I_2 when the correct answer is I_1, choosing I_2 when the correct answer is I_2) are $1-\alpha = \int_0^z P_1(n)dn$ and $1-\beta = \int_0^z P_2(n)dn$, respectively. Therefore, by applying this procedure to all different independent single samples in which the two stimuli I_1 and I_2 occur with equal probability, the overall probability of making a correct choice with the even chain $\{\sigma^{j_1} \to \ldots \to \sigma^{j_m}\}$, i.e., the hit rate is given by

$$A = \frac{1}{2}(\alpha + 1 - \beta) = \frac{1}{2}\left(\int_z^\infty P_1(n)dn + \int_0^z P_2(n)dn\right)$$
$$= \frac{1}{2}\int_0^\infty \max\big(P_1(n), P_2(n)\big)dn,$$

and the false alarm rate is

$$B = 1 - A = \frac{1}{2}(1 - \alpha + \beta)$$
$$= \frac{1}{2}\int_0^\infty \min\big(P_1(n), P_2(n)\big)dn.$$

With A and B in hand, we measure the separation between the two distributions by using the information

ratio, which is defined as $I_{I_1,I_2}^{\sigma^{j_1}\to\ldots\to\sigma^{j_m}} \equiv A/B$. The information ratio is equal to one if the two distributions totally overlap (i.e., $A = B = \frac{1}{2}$), and it approaches to $+\infty$ when the two distributions are totally separated (i.e., $A = 1, B = 0$). Therefore, when we classify the stimulus by using the occurrence count of every event chain within an event tree, the "vote" of each contributing event chain for either stimulus I_1 or I_2 is weighted with the factor $\log\left(I_{I_1,I_2}^{\sigma^{j_1}\to\ldots\to\sigma^{j_m}}\right)$. Then the weighted votes across the entire event tree are summed up to determine the candidate stimulus underlying the sample observation. This is similar to the concept of entropy in the information theory. For instance, if there are total N_c event chains within an event tree and the vote of each chain $\mathscr{C}_i$ is denoted by v_i, which takes either value $+1$ for stimulus I_1 or -1 for I_2, the summed vote v_s is given by

$$v_s = \sum_{i=1}^{N_c} v_i \log\left(I_{I_1,I_2}^{\mathscr{C}_i}\right).$$

We choose I_1 if $v_s > 0$, otherwise we choose I_2. If the two distributions of an event chain $\mathscr{C}_i$ totally merge, its vote is void because its weight $\log\left(I_{I_1,I_2}^{\mathscr{C}_i}\right) = 0$. Thus, the final choice is made by the votes with relatively significant weights.

Finally, we apply the above procedure with the information of the entire tree to all different independent single samples. In a similar way as defining the hit rate above, the discriminability of the event tree is defined as the percentage of sample observations that were correctly classified under our voting procedure (choosing I_1 when the correct answer is I_1, choosing I_2 when the correct answer is I_2). The formula is given by $D = N_{\text{correct}}/N_{\text{sample}}$ where N_{sample} is the total number of sample observations and N_{correct} is the number of times of making correct choices. In Figs. 10–13 in Section 4.2, we present the results by showing the discriminability as a function of $m_{\max}$.

References

Abraham, N. M., et al. (2004). Maintaining accuracy at the expense of speed: Stimulus similarity defines odor discrimination time in mice. *Neuron, 44*, 865–876.

Cai, D., Rangan, A. V., & McLaughlin, D. W. (2005). Architectural and synaptic mechanisms underlying coherent spontaneous activity in v1. *Proceedings of the National Academy of Sciences of the United States of America, 102*, 5868–5873.

Dayan, P., & Abbott, L. F. (2001). *Theoretical neuroscience: Computational and mathematical modeling of neural systems.* Cambridge, MA: MIT Press.

Gardiner, C. W. (1998). *A handbook of stochastic methods.* Berlin: Springer.

Gear, C. W. (1971). *Numerical initial value problems in ordinary differential equations.* Englewood Cliffs, NJ: Prentice Hall.

Hansel, D., Mato, G., Meunier, C., & Neltner, L. (1998) On numerical simulations of integrate-and-fire neural networks. *Neural Computation, 10*, 467–483.

Hodgkin, A. L., & Huxley, A. F. (1952). A quantitative description of membrane current and its application to conduction and excitation in nerve. *Journal of Physiology, 117*, 500–544.

Litvak, V., Sompolinsky, H., Segev, I., & Abeles, M. (2003). On the transmission of rate code in long feedforward networks with excitatory–inhibitory balance. *Journal of Neuroscience, 23*, 3006–3015.

Mainen, Z. F. (2006). Behavioral analysis of olfactory coding and computation in rodents. *Current Opinion in Neurobiology, 16*, 429–434.

Mattia, M., & Del Giudice, P. (2000). Efficient event-driven simulation of large networks of spiking neurons and dynamical synapses. *Neural Computation, 12*, 2305–2329.

McLaughlin, D., Shapley, R., Shelley, M., & Wielaard, J. (2000). A neuronal network model of macaque primary visual cortex (V1): Orientation selectivity and dynamics in the input layer 4Cα. *Proceedings of the National Academy of Sciences of the United States of America, 97*, 8087–8092.

Rangan, A. V., & Cai, D. (2007). Fast numerical methods for simulating large-scale integrate-and-fire neuronal networks. *Journal of Computational Neuroscience, 22*, 81–100.

Rangan, A. V., Cai, D., & McLaughlin D. W. (2005). Modeling the spatiotemporal cortical activity associated with the line-motion illusion in primary visual cortex. *Proceedings of the National Academy of Sciences of the United States of America, 102*, 18793–18800.

Rangan, A. V., Cai, D., & McLaughlin, D. W. (2008). Quantifying neuronal network dynamics through coarse-grained event trees. *Proceedings of the National Academy of Sciences of the United States of America, 105*, 10990–10995.

Reutimann, J., Giugliano, M., & Fusi, S. (2003). Event-based simulation of spiking neurons with stochastic dynamics. *Neural Computation, 15*, 811–830.

Roitman, J. D., & Shadlen, M. N. (2002). Response of neurons in the lateral intraparietal area during a combined visual discrimination reaction time task. *Journal of Neuroscience, 22*, 9475–9489.

Rousselet, G. A., Mace, M. J., & Fabre-Thorpe, M. (2003). Is it an animal? Is it a human face? Fast processing in upright and inverted natural scenes. *Journal of Visualization, 3*, 440–455.

Rudolph, M., & Destexhe, A. (2007). How much can we trust neural simulation strategies? *Neurocomputing, 70*, 1966–1969.

Schuster, H. G., & Just, W. (2005). *Deterministic Chaos.* Weinheim: Wiley-VCH Verlag.

Shadlen, M. N., & Newsome, W. T. (1998). The variable discharge of cortical neurons: Implications for connectivity, computation, and information coding. *Journal of Neuroscience, 18*, 3870–3896.

Shelley, M. J., & Tao, L. (2001). Efficient and accurate time-stepping schemes for integrate-and-fire neuronal networks. *Journal of Computational Neuroscience, 11*, 111–119.

Somers, D., Nelson, S., & Sur, M. (1995). An emergent model of orientation selectivity in cat visual cortical simple cells. *Journal of Neuroscience, 15*, 5448–5465.

Sun, Y., Zhou, D., Rangan, A. V., & Cai, D. (2009). Library-based numerical reduction of the Hodgkin-Huxley neuron for network simulation. *Journal of Computational Neuroscience, 27*, 369–390.

Sun, Y., Zhou, D., Rangan, A. V., & Cai, D. (2010). Pseudo-Lyapunov exponents and predictability of HH neuronal network dynamics. *Journal of Computational Neuroscience, 28*, 247–266.

Thorpe, S. J., & Gautrais, J. (1998). Rank order coding. In: J. Bower (Ed.), *Computational neuroscience: Trends in research* (pp. 113–119). New York: Plenum.

Troyer, T., Krukowski, A., Priebe, N., & Miller, K. (1998). Contrast invariant orientation tuning in cat visual cortex with feedforward tuning and correlation based intracortical connectivity. *Journal of Neuroscience, 18*, 5908–5927.

Uchida, N., & Mainen, Z. F. (2003). Speed and accuracy of olfactory discrimination in the rat. *Nature Neuroscience, 6*, 1224–1229.

Uchida, N., Kepecs, A., & Mainen, Z. F. (2006). Seeing at a glance, smelling in a whiff: Rapid forms of perceptual decision making. *Nature Reviews. Neuroscience, 7*, 485–491.

Victor, J. D., & Purpura, K. P. (1997). Sensory coding in cortical neurons: Recent results and speculations. *Annals of the New York Academy of Sciences, 835*, 330–352.